PHYSICAL REVIEW B **83**, 144410 (2011)

Iron-vacancy superstructure and possible room-temperature antiferromagnetic order in superconducting $Cs_yFe_{2-x}Se_2$

V. Yu. Pomjakushin and D. V. Sheptyakov
Laboratory for Neutron Scattering, Paul Scherrer Institut, CH-5232 Villigen PSI, Switzerland

E. V. Pomjakushina, A. Krzton-Maziopa, and K. Conder
Laboratory for Developments and Methods, PSI, CH-5232 Villigen PSI, Switzerland

D. Chernyshov and V. Svitlyk
Swiss-Norwegian Beam Lines at ESRF, BP220, F-38043 Grenoble, France

Z. Shermadini
Laboratory for Muon Spin Spectroscopy, Paul Scherrer Institut, CH-5232 Villigen PSI, Switzerland
(Received 9 February 2011; revised manuscript received 17 March 2011; published 14 April 2011)

Neutron and x-ray powder and single crystal synchrotron diffraction of $Cs_yFe_{2-x}Se_2$ show the presence of superstructure reflections with propagation vector $k = [\frac{2}{5}, \frac{1}{5}, 1]$ with respect to the average crystal structure $I4/mmm$ ($a \sim 4$, $c \sim 15$ Å). The propagation vector star corresponds to the 5 times bigger unit cell given by transformation $\mathbf{A} = 2\mathbf{a} + \mathbf{b}$, $\mathbf{B} = -\mathbf{a} + 2\mathbf{b}$, $\mathbf{C} = \mathbf{c}$. A solution for the atomic structure is found in the space group $I4/m$ with an ordered pattern of iron vacancies corresponding to the iron deficiency $x = 0.29$ and Cs stoichiometry $y = 0.83$. The superstructure satellites are more pronounced in the neutron diffraction patterns suggesting that they can have some magnetic contribution. We have sorted out all possible symmetry adapted magnetic configurations and found that the presence of antiferromagnetic ordering with the ordered magnetic moment of Fe with $\simeq 2\mu_B$ does not contradict the experimental data. However, the solutions space is highly degenerate and we cannot choose a specific solution. Instead we propose possible magnetic configurations with the Fe magnetic moments in (ab) plane or along c axis. The superstructure is destroyed above $T_s \simeq 500$ K by a first-order-like transition.

DOI: 10.1103/PhysRevB.83.144410 PACS number(s): 75.50.Ee, 75.25.−j, 61.05.C−, 74.90.+n

I. INTRODUCTION

The recent discovery of Fe-based superconductors has triggered a remarkable renewed interest for possible new routes leading to high-temperature superconductivity. As observed in the cuprates, the iron-based superconductors exhibit interplay between magnetism and superconductivity suggesting the possible occurrence of unconventional superconducting states. Other common properties are the layered structure and the low carrier density. Among the iron-based superconductors FeSe has the simplest structure with layers in which Fe cations are tetrahedrally coordinated by Se.[1] Recently superconductivity at about 30 K was found in $X_yFe_{2-x}Se_2$ for X = K, Cs, and Rb.[2–4] Muon-spin rotation/relaxation (μSR) experiments show that the superconducting state observed in $Cs_yFe_{2-x}Se_2$ below 28.5(2) K is microscopically coexisting with a magnetic phase with a transition temperature at $T_m = 478.5(3)$ K.[5] The magnetic phase appears characterized by rather large static iron moments as the μSR signal is wiped out below T_m. Very recently the AFM order was reported[6] in superconducting $K_{0.8}Fe_{1.6}Se_2$ with $T_N = 560$ K with the iron magnetic moment $3.31\mu_B$.

The average crystal structure of $X_yFe_{2-x}Se_2$ is the same as in the layered (122-type) iron pnictides with the space group $I4/mmm$.[7] Different types of iron vacancy ordering in $Tl_yFe_{2-x}Se_2$ were observed long time ago,[8–10] including the one with a 5 times bigger unit cell. Due to a renewed interest in the superconducting chalcogenides, many new experimental studies on the vacancy ordering in $X_yFe_{2-x}Se_2$ (X = K, Tl) have appeared very recently.[6,11–14]

In the present paper we report on the observation of superstructure in superconducting ($T_c = 28.5$ K) $Cs_yFe_{2-x}Se_2$ below $T_s \simeq 500$ K and analyze the diffraction data assuming iron vacancy ordering and possible antiferromagnetic ordering of Fe at room temperature. The single crystals used in the present study are the same as in Refs. 3 and 5.

II. EXPERIMENTAL DETAILS

Single crystals of cesium intercalated iron selenides of nominal compositions $Cs_{0.8}(FeSe_{0.98})_2$ were grown from the melt using the Bridgman method as described in Ref. 3. Powder x-ray diffraction was performed using a D8 Advance Bruker AXS diffractometer with CuK_α radiation. For these measurements a fraction of the crystal was cleaved, powdered, and loaded into the low background airtight specimen holder in a He-glove box to protect the powder from oxidation. Differential scanning calorimetry (DSC) experiments were performed with a Netzsch DSC 204F1 system. Measurements were performed on heating and cooling with a rate of 10 K/min using 20 mg samples encapsulated in standard Al crucibles. An argon stream was used during the whole experiment as a protecting gas. Neutron powder diffraction experiments were carried out at the SINQ spallation source of Paul Scherrer Institute (Switzerland) using the high-resolution diffractometer for thermal neutrons HRPT[15] ($\lambda = 1.866, 1.494$ Å, high

intensity mode $\Delta d/d \geqslant 1.8 \times 10^{-3}$). Refinement of crystal and magnetic structures from powder neutron diffraction data were carried out with FULLPROF[16] program, with the use of its internal tables for scattering lengths and magnetic form factors. Single crystal diffraction data were collected at the SNBL beamline BM1A at the ESRF synchrotron in Grenoble (France) with a MAR345 image-plate area detector using $\lambda = 0.6977(1)$ Å. Intensities were indexed and integrated with CrysAlis,[17] empirical absorption correction was made with SADABS,[18] and structure refinement with SHELXL97.[19]

III. RESULTS AND DISCUSSION

The average crystal structure can be refined in the standard structure model.[3] The iron site occupancy is refined to smaller than unity for both x-ray and neutron diffraction data indicating the presence of the vacancies on the iron sites. The structure parameters refined in this model are presented in Table I for both laboratory x-ray and NPD data. The neutron diffraction pattern has a set of extra diffraction peaks that can be indexed with the propagation k vector $k = [\frac{2}{5}, \frac{1}{5}, 1]$ (as shown in Fig. 1). To obtain Fig. 1 we first made the refinement in the $I4/mmm$ average structure model that resulted in the structure parameters shown in the second column of Table I. Then we fixed all the parameters including the scale factor and background parameters and added the second phase describing the satellites with $\pm k$ and performed the profile matching Lebail fit, in which the integral peak intensities are the refined parameters. However the x-ray powder diffraction pattern contains only one clearly visible satellite $(\frac{3}{5}, -\frac{1}{5}, 0)$ at $q = 1$ Å^{-1}, which allows one to suggest that the satellites seen by neutron might have magnetic contribution. The propagation vector star $k = \{[\frac{2}{5}, \frac{1}{5}, \pm 1], [-\frac{2}{5}, -\frac{1}{5}, \pm 1], [\frac{1}{5}, -\frac{2}{5}, \pm 1], [-\frac{1}{5}, \frac{2}{5}, \pm 1]\}$ corresponds to the new unit cell given by the transformation $\mathbf{A} = 2\mathbf{a} + \mathbf{b}$, $\mathbf{B} = -\mathbf{a} + 2\mathbf{b}$, $\mathbf{C} = \mathbf{c}$ (the illustration of the lattice cell transformation is shown in Fig. 2). A good refinement of NPD pattern explaining the satellite peaks can be done with the supercell indicated above in the space groups $P4_2/n$ and $I4/m$. Using the fixed new atomic positions generated from the average crystal structure ($I4/mmm$) by applying the above basis transformation and releasing only the site occupancies and z-Se, similar to the average structure, one immediately gets a reasonably good description of the superstructure peaks. Table I shows the atomic positions and details of the refinements. The Fe site splits in two sites in $I4/m$ (no. 87) and in three sites in $P4_2/n$ [no. 86, note to work in the second setting with origin at -1 post-matrix translation $(\frac{1}{4}, \frac{1}{4}, \frac{1}{4})$ should be applied]. Both groups give similar quality of the refinements of the single crystal data as we explain below, so we present the results only for the $I4/m$ space group, which is more symmetric with respect to the iron sites. The atomic positions for the $I4/m$ space group generated by the above transformation from average space group $I4/mmm$ are listed in Table I. All "symmetric" positional parameters which were generated from the coordinates of special positions of $I4/mmm$ were fixed in the refinement. The fully occupied Fe1 (16i) site contributes 1.6 of iron stoichiometry in $Cs_yFe_{2-x}Se_2$. If both site occupancies are refined, Fe1 gets almost maximal value, whereas Fe2 (4d) site occupancy is close to zero, as shown in Table I. The iron vacancy pattern looks like the one shown in Fig. 2.

Since both vacancy superstructure and possible magnetic structure with $k = 0$ contribute to the same neutron

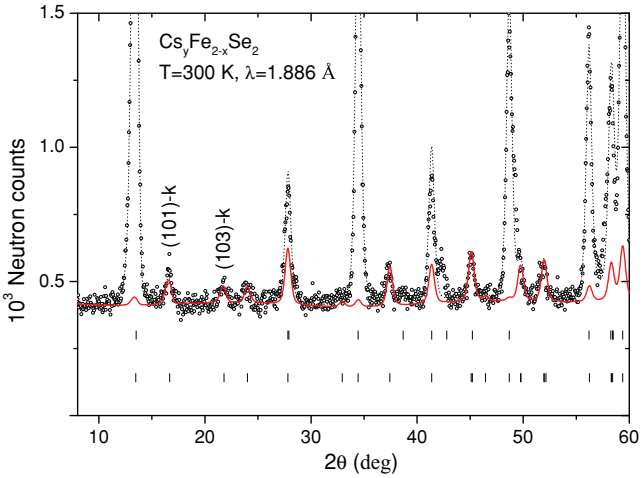

FIG. 1. (Color online) Fragment of the neutron diffraction pattern of $Cs_yFe_{2-x}Se_2$ at room temperature. Contribution of the superstructure peaks refined in the powder profile matching Lebail mode for $k = [\frac{2}{5}, \frac{1}{5}, 1]$ with respect to the average crystal structure ($I4/mmm$ with $a = 3.96$, $c = 15.29$ Å, and the structure parameters fixed by the values shown in the second column of Table I) is shown by the red solid curve. The upper row of tics indicates the Bragg peak positions from the average structure and the lower hashmarks indicate reflections associated the propagation vectors $\pm k$.

TABLE I. Crystal structure parameters refined in the average structure model $I4/mmm$ (no. 139), Fe in $(0, \frac{1}{2}, \frac{1}{4})$ (4d), Se in $(0,0,z)$ (4e), and Cs in (0,0,0) (2a) positions. In the space group $I4/m$ (no. 87), whose unit cell is generated by the transformation given in the text, the atoms are split in the following way: Cs in (0,0,0) (2a) and (0.4,0.8,0) (8h), Se in $(0.4,0.8, -z_{Se})$ (16i) and $(\frac{1}{2}, \frac{1}{2}, -z_{Se} + \frac{1}{2})$ (4e), and Fe in (0.3,0.6,0.25) (16i) and $(\frac{1}{2}, 0, \frac{1}{4})$ (4d), where z_{Se} is a z component in $I4/mmm$. The stoichiometries o-Cs and o-Se are calculated to be in units of the formula $Cs_yFe_{2-x}Se_2$. The data for laboratory x-ray and neutron powder diffraction NPD are given at room temperature. The structure parameters from the synchrotron single crystal (s.c.) experiment are at $T = 536$ K for true $I4/mmm$ symmetry above the order-disorder transition.

	X-ray 300 K	NPD 300 K	NPD, $I4/m$ 300 K	s.c. x-ray 536 K
a	3.9608(2)	3.9614(2)	8.8582(3)	4.0177(5)
c	15.285(1)	15.2873(9)	15.2873(9)	15.333(4)
z-Se	0.3456(4)	0.3436(3)	−0.343(3)	0.3443(3)
o-Cs	0.636(13)	0.622(24)	0.73(1)	0.754(9)
o-Fe1	1.48(3)	1.49(3)	1.50(2)	1.66(8)
o-Fe2			0.024(8)	
B-Fe	1.4(3)	1.7(1)	2.1(1)	1.3(2)
B-Se	4.3(2)	3.6(1)	3.2(1)	1.2(2)
B-Cs	2.6(3)	4.8(5)	5.9(5)	3.2(2)
R_{wp} (%)	5.95	7.47	7.12	21
χ^2	3.6	3.3	2.86	1.4

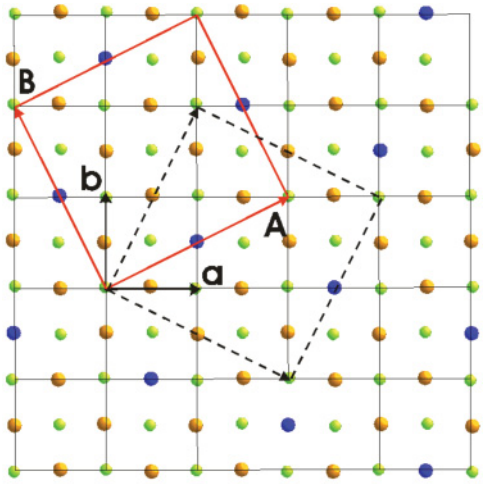

FIG. 2. (Color online) The lattice unit cell transformation to a new bigger tetragonal supercell shown by capital letters. The supercell shown by solid red lines corresponds to the propagation vector star generated by $\mathbf{k}_1 = [\frac{2}{5}, \frac{1}{5}, 1]$. The dashed cell shows the twin domain that corresponds to the star generated by $\mathbf{k}_2 = [\frac{1}{5}, \frac{2}{5}, 1]$. The k-vector stars are shown in Fig. 3. Iron vacancy ordering pattern in the ab plane is shown by blue circles. The brown and green circles show fully occupied Fe and Se positions projected to the ab plane.

Bragg peaks, one needs the reliable crystal structure data to disentangle possible magnetic contribution. For this purpose several data sets were collected in the single crystal x-ray synchrotron experiment at room temperature and at 536 K above T_m and T_s. In addition, a limited slice of reciprocal space around $(-\frac{2}{5}, -\frac{4}{5}, 0)$ satellite was collected at heating to identify the transition. Figure 3 shows a slice of the reciprocal space near the $[hk0]$ plane. The superstructure reflections belonging to two twin domains as shown in Fig. 3 can be easily identified (the twin populations are 57.6% /42.4%).

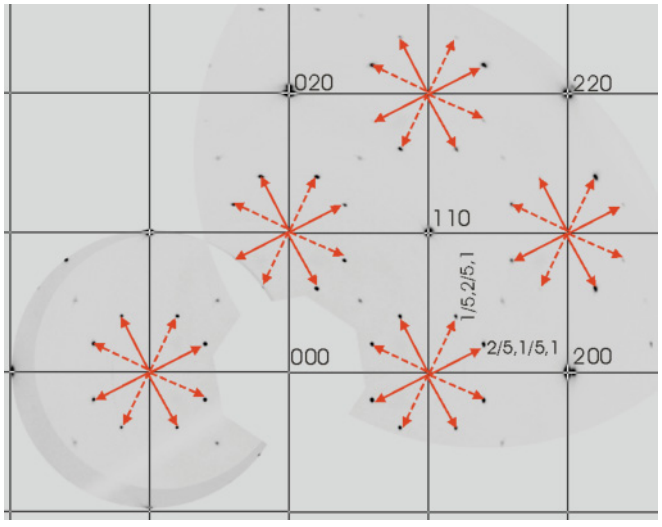

FIG. 3. (Color online) A slice of the reciprocal space showing $[hk0]$ plane at room temperature. The indexing is given in the average cell ($I4/mmm$). The satellite reflections are indicated by red arrows for $\mathbf{k}_1 = [\frac{2}{5}, \frac{1}{5}, 1]$ and $\mathbf{k}_2 = [\frac{1}{5}, \frac{2}{5}, 1]$ by solid and dashed lines, respectively. These two k vectors correspond to two twin domains shown in Fig. 2.

TABLE II. Crystal structure parameters refined in the space group $I4/m$ (no. 87) from the synchrotron single crystal experiment at room temperature. The Wyckoff site symmetry positions are the same as described in the caption of Table I. The refined stoichiometry is $Cs_{0.83(1)}Fe_{1.71(1)}Se_2$, The Fe1 site occupancy was fixed to 1. Anisotropic atomic displacement parameters U_{ij} are in Å^2 multiplied by 10^3. U_{eq} is defined as one third of the trace of the orthogonalized U_{ij} tensor. Forty parameters were refined using 6286 reflections, 539 of which are independent. Final R factors are $R1 = 0.0860$, $wR2 = 0.1955$ $[I > 2\sigma(I)]$ and $R1 = 0.0940$, $wR2 = 0.2105$ (all data).

	$x\ y\ z$	U_{iso}	occ
Cs1	0.0000 0.0000 0.0000	78(2)	0.911(14)
Cs2	0.4041(2) 0.8057(2) 0.000	75(2)	0.81(1)
Se1	0.3924(2) 0.7987(2) 0.6551(2)	55(2)	1
Se2	0.5000 0.5000 0.1488(2)	54(2)	1
Fe1	0.3014(1) 0.5938(1) 0.25165(6)	59(2)	1
Fe2	0.5000 0.0000 0.2500	56(9)	0.27(2)

	U_{11}	U_{22}	U_{33}	U_{23}	U_{13}	U_{12}
Cs1	92(2)	92(2)	49(4)	0	0	0
Cs2	84(2)	93(2)	49(3)	0	0	3.9(7)
Se1	61(2)	59(2)	45(2)	2.1(5)	1.1(5)	1.6(5)
Se2	58(2)	58(2)	44(3)	0	0	0
Fe1	63(3)	62(2)	51(4)	0.8(7)	−1.1(6)	−0.1(7)
Fe2	62(10)	62(10)	45(16)	0	0	0

The angle between the domains amounted to 53.13(5) deg in accordance with the drawing of Fig. 2 predicting the angle $2 \arctan \frac{1}{2} = 53.130$ deg. Note that the extra peaks are centered around forbidden nodes because they are satellites of the Bragg peaks from the adjacent $[hk1]$ and $[hk-1]$ planes. The refined structure parameters together with the reliability factors are given in Table II. Due to the strong absorption correction effects, the atomic displacement parameters (ADP) can have an overall systematic shift. The refinement of the single crystal data in the $P4_2/n$ space group also gives acceptable reliability factors that we list here for completeness: $R1 = 0.0860$, $wR2 = 0.2131$ $[I > 2\sigma(I)]$, and $R1 = 0.1283$, $wR2 = 0.2885$ (all data).

One can notice additional diffraction spots at $(\frac{n}{2}, \frac{m}{2}, 0)$ in Fig. 3. The inspection of the reciprocal space sliced along the c direction shows that these spots are actually a projection of satellite rods at $(\frac{n}{2}, \frac{m}{2}, l)$. The in-plane propagation vector is equal to $[\frac{1}{2}, \frac{1}{2}]$ in both average cell and supercell. We do not have any model to account for this additional superstructure, but it must correspond to a 2D ordering within the (ab) plane, for example, an ordering of vacancies in Cs layers without correlations between the layers along the c axis.

Using the structure data for $I4/m$ from the single crystal x-ray experiment we made an attempt to evaluate the magnetic contribution in the NPD data. We assume that only the fully occupied Fe1 site has a magnetic moment. All the structure parameters from Table II were fixed in the subsequent NPD refinements. Only overall ADP was introduced to account for the absorption effects in the x-ray experiment. The space group $I4/m$ has eight one-dimensional irreducible representations (irreps) for $k = 0$, and all eight irreps enter three times in

TABLE III. Irreps τ_i, $i = 1,\ldots,8$ of the space group $I4/m$ (no. 87) for k vector $k = 0$. Numeration of the irreps is in accordance with the Kovalev book ($k = k_{14}$, Table $T121$).[20] $\tau_4 = \tau_3\tau_2$, $\tau_6 = \tau_5\tau_2$, $\tau_8 = \tau_7\tau_2$. The basis functions ψ for the spin of iron atom in general (16i) position for τ_4 [two in (ab) plane] and for τ_7 (one along c axis) are given for the illustration of possible magnetic structures.

	h_1	h_{14}	h_4	h_{15}	h_{25}	h_{38}	h_{28}	h_{39}
τ,ψ	1	4_z^+	2_z	4_z^-	-1	-4_z^+	m_z	-4_z^-
τ_2	1	1	1	1	-1	-1	-1	-1
τ_3	1	i	-1	$-i$	1	i	-1	$-i$
τ_5	1	-1	1	-1	1	-1	1	-1
τ_7	1	$-i$	-1	i	1	$-i$	-1	i
ψ_4, ab	1,0	0,$-i$	1,0	0,$-i$	-1,0	-1,0	0,i	0,i
ψ_4, ab	0,1	i,0	0,1	i,0	0,-1	0,-1	$-i$,0	$-i$,0
ψ_7, c	1	i	-1	$-i$	1	i	-1	$-i$

the magnetic representation for the iron in the general (16i) position. The irreps in Kovalev notation[20] are listed in Table III. There are four real irreps that correspond to the respective Shubnikov groups of $I4/m$ and four complex irreps with Herring criterion 0 that do not have a Shubnikov counterpart. We sorted out all the irreps and found that there are different magnetic configurations with the moment size about $2\mu_B$ per iron site that do not contradict the NPD data. The magnetic R factors amounted to 17.5% –24.5% for different irreps. For the illustration of the magnetic contribution we show in Table III and in Fig. 4 two "orthogonal" magnetic models. For τ_4 we choose the basis functions with the moments in the (ab) plane, whereas for τ_7 the moments are parallel to the c axis. Both models have practically the same magnetic Bragg R factors 18.5% and 17.5%, respectively. The τ_4 predicts significantly larger intensity of (103) magnetic Bragg peak in comparison with τ_7 and τ_2 irreps. We note that the magnetic moment sizes on the Fe1 sites are not restricted to be the same by

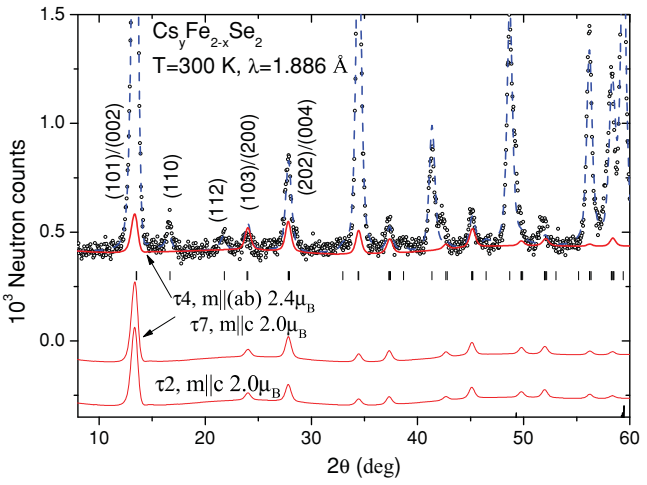

FIG. 4. (Color online) Fragment of the experimental NPD pattern and the refined profiles for three magnetic models given by symmetry adapted basis functions in the $I4/m$ space group. The full profile is shown by the dashed blue line and the solid red lines show magnetic contributions to the profile. The curves for τ_7 and τ_2 are shifted along y axis for better visibility. See text for details.

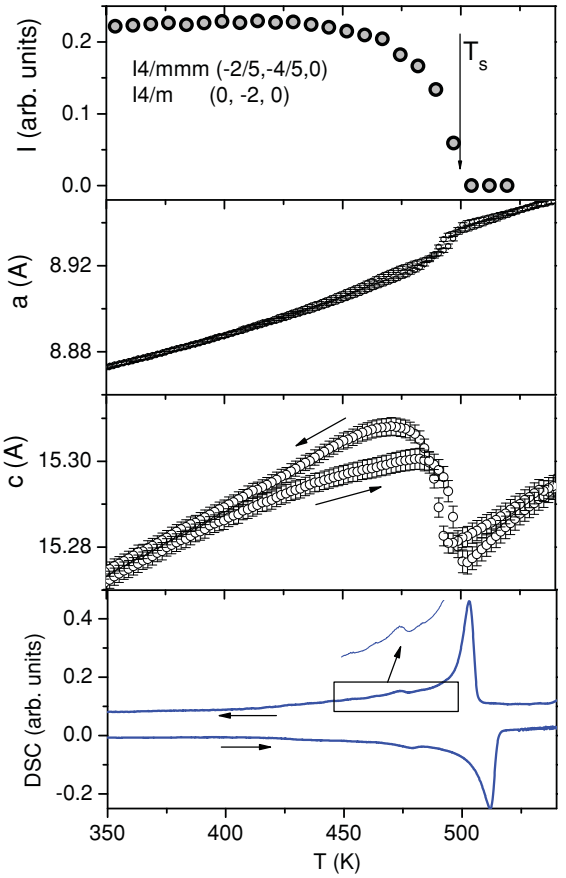

FIG. 5. (Color online) Integrated intensity of (0,−2,0) superstructure satellite, lattice constants obtained from the synchrotron measurements and differential scanning calorimetry (DSC) signal as a function of temperature. The superstructure satellite intensity was obtained from the single crystal measurement on heating. The lattice constants were refined from powder diffraction synchrotron data both on heating and cooling.

symmetry for complex irreps even if we consider the basis function only along one axis. For instance, ψ_7 can be multiplied by an arbitrary phase factor $\exp(i\varphi)$ that would result in two different moment values. By choosing the phase $\varphi = \pi/4$ all the moments are constrained to be the same.

The model proposed in Ref. 6 corresponds to τ_2 with the Shubnikov symbol $I4/m'$. Unfortunately we do not observe an explicit magnetic contributions in the (101) Bragg peak as observed in Ref. 6 in K-intercalated FeSe . This might be partially due to the fact that for the lattice constants of $Cs_yFe_{2-x}Se_2$ the (101) and (002) appear at almost identical scattering angles. In addition, in our case of $Cs_yFe_{2-x}Se_2$ the magnetic contribution seems to be not so large. For comparison we also show the contribution of this model (τ_2,||c) to the diffraction pattern (Fig. 4). One can see that the contributions of both τ_7 and τ_2 models are very similar (there are small differences hardly visible on the figure scale, $R_{\text{Bragg}} = 18.5\%$ for τ_2), but the magnetic configurations are different, namely for τ_7 the constant moment configuration corresponding to the operators listed in the table are 1,−1,−1,1,1,−1,−1,1, whereas for τ_2 1,1,1,1,−1,−1,−1,−1. Probably the τ_7 model would also fit the data of Ref. 6. We would like to stress that the possible solutions are highly degenerate by the values of the R factors

and we cannot choose a specific model on the basis of our experimental data. Interestingly to note that τ_7 and τ_2 solutions are predicted by recent first-principles calculation on the same material[21] where the τ_2 structure is called "block spin" and is the lowest energy configuration, and the τ_7 structure is called "zig-zag collinear" and is the second lowest energy configuration.

Figure 5 shows the integrated intensity of the superstructure satellite and the lattice constants as a function of temperature obtained in the single crystal and powder synchrotron diffraction experiments. The intensity gradually disappears with transition temperature $T_s \simeq 500$ K, whereas the lattice constants exhibit a pronounced hysteresis indicating a first-order phase transition. The unit cell volume is linear and does not have a visible peculiarity in the temperature region shown in Fig. 5. Interestingly, the c-lattice constant shows a decrease by 0.1% at the transition to the disordered phase. The crystal structure above T_s is well refined in the $I4/mmm$ model (Table I). The DSC signal has two peaks, one large at higher temperature and the second small one at lower temperature, which had been associated with the onset of the magnetic order from the μSR experiment.[5] The large DSC peak seems to be originating from the vacancy order-disorder transition at $T_s \simeq 500$ K.

ACKNOWLEDGMENTS

The authors acknowledge the allocation of the beam time at Swiss-Norwegian beam line (BM1A) of the European Synchrotron Radiation Facility (ESRF, Grenoble, France). Fruitful discussions with A. Bosak are gratefully acknowledged. The authors thank the NCCR MaNEP project and Sciex-NMS^{ch} (Project Code 10.048) for the support of this study. The work was partially performed at the neutron spallation source SINQ.

[1] F.-C. Hsu *et al.*, Proc. Natl. Acad. Sci. USA **105**, 14262 (2008).
[2] J. Guo, S. Jin, G. Wang, S. Wang, K. Zhu, T. Zhou, M. He, and X. Chen, Phys. Rev. B **82**, 180520 (2010).
[3] A. Krzton-Maziopa, Z. Shermadini, E. Pomjakushina, V. Pomjakushin, M. Bendele, A. Amato, R. Khasanov, H. Luetkens, and K. Conder, J. Phys. Condens. Matter **23**, 052203 (2011), URL [http://stacks.iop.org/0953-8984/23/i=5/a=052203].
[4] A. F. Wang *et al.*, Phys. Rev. B **83**, 060512 (2011).
[5] Z. Shermadini *et al.*, Phys. Rev. Lett. **106**, 117602 (2011).
[6] W. Bao, Q. Huang, G. F. Chen, M. A. Green, D. M. Wang, J. B. He, X. Q. Wang, and Y. Qiu, e-print arXiv:1102.0830.
[7] M. Rotter, M. Tegel, and D. Johrendt, Phys. Rev. Lett. **101**, 107006 (2008).
[8] L. Haggstrom, H. Verma, S. Bjarman, R. Wappling, and R. Berger, J. Solid State Chem. **63**, 401 (1986).
[9] H. Sabrowsky, M. Rosenberg, D. Welz, P. Deppe, and W. Schafer, J. Magn. Magn. Mater. **54-7**, 1497 (1986).
[10] L. Haggstrom, A. Seidel, and R. Berger, J. Magn. Magn. Mater. **98**, 37 (1991).
[11] M. Fang, H. Wang, C. Dong, Z. Li, C. Feng, J. Chen, and H. Q. Yuan, e-print arXiv:1012.5236.
[12] Z. Wang, Y. J. Song, H. L. Shi, Z. W. Wang, Z. Chen, H. F. Tian, G. F. Chen, J. G. Guo, H. X. Yang, and J. Q. Li, e-print arXiv:1101.2059.
[13] P. Zavalij *et al.*, e-print arXiv:1101.4882v1.
[14] J. Bacsa, A. Y. Ganin, Y. Takabayashi, K. E. Christensen, K. Prassides, M. J. Rosseinsky, and J. B. Claridge, e-print arXiv:1102.0488.
[15] P. Fischer *et al.*, Physica B **276–278**, 146 (2000).
[16] J. Rodriguez-Carvajal, Physica B **192**, 55 (1993).
[17] CRYSALIS Software System, Ver. 1.171.31.4 (Oxford-diffraction Ltd., Oxford, England, 2006).
[18] G. M. Sheldrick, SADABS, Version 2.06 (University of Goettingen, Germany, 2002).
[19] G. M. Sheldrick, SHELXL97 (University of Goettingen, Germany, 1997).
[20] O. V. Kovalev, *Representations of the Crystallographic Space Groups: Irreducible Representations, Induced Representations, and Corepresentations*, 2nd ed. (Gordon and Breach, New York, 1993).
[21] C. Cao and J. Dai, e-print arXiv:1102.1344.